Send Orders for Reprints to reprints@benthamscience.ae

Current Nanoscience, 2017, *13*, 1-9

RESEARCH ARTICLE

Photocatalytic Reduction of Aqueous Mercury (II) Using Hybrid WO_3-TiO_2 Nanotubes Film

Wai Hong Lee[1], Swe Jyan Teh[1], Pui May Chou[2] and Chin Wei Lai[1,*]

[1]*Nanotechnology & Catalysis Research Centre (NANOCAT), 3rd Floor, Block A, Institute of Postgraduate Studies (IPS), University of Malaya, 50603 Kuala Lumpur, Malaysia;* [2]*School of Engineering, Taylor's University Lakeside Campus, No. 1, Jalan Taylor's, 47500 Subang Jaya, Selangor Darul Ehsan, Malaysia*

ARTICLE HISTORY

Received: April 19, 2017
Revised: May 25, 2017
Accepted: June 5, 2017

DOI:
10.2174/1573413713666170616084447

Abstract: ***Background*:** Mercury pollution has become a serious and enduring threat to the environment. It has affected the organisms along the food chain, including humans. Thus, it is necessary to design an effective mercury removal system to overcome the huge threat of mercury pollution. Our study aim is to optimize the anodization duration of as-prepared WO_3-loaded TiO_2 nanotubes for improving their photocatalytic mercury (II) reduction performance.

***Methods*:** Hybrid WO_3-TiO_2 nanotubes film were successfully formed via electrochemical anodization at applied potential of 40 V in ethylene glycol organic electrolyte containing 1 vol% of hydrogen peroxide (H_2O_2) and 0.3 wt% ammonium fluoride (NH_4F) by varying the anodization time from 15 up to 120 minutes. A tungsten electrode was chosen as the cathode as an innovative and convenient approach to hybridize WO_3 with TiO_2 nanotubes film

***Results*:** During electrochemical anodization, W6+ ions dissolve from the cathode into the electrolyte solution, migrate towards the titanium foil and are deposited evenly on the Ti foil. This study recorded a maximum photocatalytic mercury (II) reduction performance of 91% (with exposure to 96 W UV-B Germicidal light irradiation for 120 minutes) in the presence of WO_3-$_{TiO2}$ nanotubes film with the highest aspect ratio (53.04) and geometric surface area factor (345.68).

***Conclusion*:** The main reason might be attributed to the high specific surface area nanotubes architecture performed strong light scattering effects as well as better incident light absorption from any direction to trigger more charge carriers for photocatalytic reduction of mercury(II) into elemental mercury. WO_3 acted as an effective mediator to trap the photo-induced electrons from the TiO_2, by contributing intermediate energy band levels below the conduction band of TiO_2.

Keywords: WO_3-loaded TiO_2 nanotubes, anodization, aspect ratio, geometric surface area factor, photocatalytic reduction of mercury (II), electrochemical anodization.

1. INTRODUCTION

The unique properties of mercury such as low electrical resistance, high surface tension and high specific gravity, make it an attractive material option for many specialists' use and applications [1]. Due to the diverse range of applications of mercury throughout the past, mercury pollution has become a serious and enduring threat to the environment. It has affected the organisms along the food chain, including humans. Thus, it is necessary to design an effective mercury removal system to overcome the huge threat of mercury pollution [2].

Recently, titanium dioxide (TiO_2) nanotubes have been gaining widespread attention as a potential photocatalyst for heavy metal removal application [3, 4]. TiO_2 has demonstrated to be a suitable photocatalyst with unique features (non-toxic, durable, stable against corrosion, high photocatalytic activity), leading to its widespread use for the photodegradation of various pollutants [3, 5, 6]. This high activity is due to the high specific surface area of TiO_2 nanotubes which allows it to adsorb more pollutant particles. TiO_2 also effectively passivates heavy metal ions by generating reactive species under UV light illumination, which in turn reduces the heavy metal ions to inert metal oxides. Nevertheless, the photocatalytic activity of TiO_2 is constrained due to its wide band gap of 3.20 eV, which confines its light har-

*Address correspondence to this author at the Nanotechnology & Catalysis Research Centre (NANOCAT), 3rd Floor, Block A, Institute of Postgraduate Studies (IPS), University of Malaya, 50603 Kuala Lumpur, Malaysia;
Tel: +603-79676959; Ext: 2925; Fax: +603-79676556;
E-mail: cwlai@um.edu.my

1573-4137/17 $58.00+.00

vesting properties to about 4% of the solar spectrum [7]. This has led to many efforts to improve the visible light absorption of TiO_2 by coupling TiO_2 with another semiconductor to induce additional electronic state in the band gap [8].

This study reports the activity of TiO_2 nanotube films hybridized with WO_3 for enhanced photoreduction of mercury(II). WO_3 possesses a narrow band gap of 2.3-2.8 eV with strong absorption in the visible range (400-700 nm), which is advantageous for visible-light-driven photocatalysis. Hybridizing WO_3 and TiO_2 results in the formation of a type-III heterojunction due to the differences in the valence and conduction band positions. The potential gradient formed at the heterojunction allows ease of electron transfer from the conduction band of TiO_2 down to the conduction band of WO_3. Based on our preliminary studies, this modification of WO_3-loaded TiO_2 nanotubes film could further improve the excited charge carrier separation and inhibit charge carrier recombination during the photocatalytic reaction [8-10]. Therefore, our study aimed to optimize the anodization duration of as-prepared WO_3-loaded TiO_2 nanotubes for improving their photocatalytic reduction of Hg^{2+} ions.

2. METHODOLOGY

Titanium, Ti (0.127 mm, 99.6 % purity, 42.0 μΩ-cm) and tungsten foil (0.127 mm, 99.9 % purity, 4.9 μΩ-cm) were purchased from Sigma Aldrich (USA). Hydrogen peroxide, H_2O_2 and ethylene glycol were purchased from Friendemann Schmidt (Germany), whereas ammonium fluoride, NH_4F was obtained from Merck (USA). The anodization of Ti foil was carried out in a two-electrode electrochemical cell at a fixed distance of 2 cm between the two electrodes. The anode comprised of a 5 cm x 1 cm Ti foil, while tungsten foil was used as the cathode. The electrolyte solution consisted of 1 vol% H_2O_2 and 0.3 wt% NH_4F dissolved in ethylene glycol. H_2O_2 served as a sacrificial agent to increase the rate of Ti oxidation to form TiO_2 nanotubes [8, 10]. In the present study, anodization was performed at potential of 40 V for durations ranging from 15 to 120 minutes. After the anodization process, the Ti foil was cleaned by immersing in deionized water and ultrasonicated in an ultrasonic bath for 1 minute to remove the remaining electrolyte on the Ti foil and eliminate the debris and precipitation layers on top of the nanotubes [9]. The samples were then annealed in air at 400 °C for 4 hours. Based on our preliminary studies, as-anodized WO_3-loaded TiO_2 nanotubes were amorphous in nature. An annealing temperature of 400 °C for 4 hours was found to be sufficient to form the crystalline anatase phase [8-10]. Uniformly-ordered TiO_2 nanotubes with highly crystalline anatase phase offers favourable transport pathways for shifting the photo-induced electrons to WO_3 species [9].

The synthesized WO_3-hybridized TiO_2 nanotubes were then characterized using various techniques to comprehend the properties of the material. Field emission scanning electron microscopy (FESEM) was employed to observe the morphology of the WO_3-TiO_2 nanotube films (FEI Quanta 200F, FEI, USA) microanalysis at 5 kV. The phase of the WO_3-TiO_2 nanotubes was determined using X-ray diffraction (XRD, Bruker D8 Advance diffractometer, Bruker, USA) which was conducted between 10 to 80 ° with Cu Kα radiation (α = 1.5406 Å). Raman spectroscopy was performed using a 514.5 nm Ar^+ laser excitation source, which further confirmed the phase composition of the samples (Renishaw in Via, Renishaw plc, Gloucestershire, UK). The optical properties of the WO_3-loaded TiO_2 nanotube arrays were analysed with a UV-vis diffuse reflectance spectrophotometer (UV-vis DRS, Shimadzu UV-2700, Shimadzu, Kyoto, Japan) equipped with an integrating sphere. The chemical and oxidation states of the WO_3-loaded TiO_2 nanotubes were investigated using X-ray photoelectron spectroscopy (XPS, PHI Quantera II, Physical Electronics, Chanhassen, MN, USA) with an Al cathode (hv = 1486.8 eV) with 100 microns spot size and 280 eV pass energy.

The photocatalytic mercury(II) reduction performance of WO_3-TiO_2 nanotubes was carried out in a quartz glass photoreactor equipped with a TUV 96W UV-B Germicidal light source. The WO_3-TiO_2 sample was immersed in 100 mL of 100 ppb mercury chloride, $HgCl_2$ solution under dark conditions for 30 minutes for dark absorption. After dark absorption, 5 mL of solution was sampled at 0, 60 and 120 minutes of exposure for photoirradiation to determine the rate of photocatalytic mercury(II) reduction. The concentration of mercury(II) after the photocatalytic reduction by WO_3-loaded TiO_2 nanotubes was measured using a mercury analyzer (NIC RA-3120, Nippon Instruments Corporation, Osaka, Japan) [8].

3. RESULTS AND DISCUSSION

3.1. Morphological Studies and Elemental Analysis

The influence of anodization duration on the morphology of WO_3-loaded TiO_2 nanotubes was investigated in the present study. Prior to anodization, the surface of Ti foils appeared brightly polished on both sides. The surface morphologies of WO_3-loaded TiO_2 nanotubes at varying anodization times between 15 to 120 minutes are shown in Fig. (**1**). Randomly-distributed pits were observed on the surface of TiO_2 film which was anodized for 15 minutes, which may be attributed to the chemical and field-assisted dissolution of the oxide at reactive sites on the Ti surface. The measured thickness of the porous oxide layer was approximately 0.9 μm. Larger pores were observed when anodization was performed for 30 minutes, as further field-assisted dissolution of TiO_2 transformed the randomly-distributed pits into a larger pore structure. The pores eventually interconnected to form a uniform nanotubular structure with tube length of approximately 1.6 μm and average pore size of 50 nm. Increasing the anodization times was found to impact the final length of the nanotubes, which increased from 1.8 μm, 5.2 μm to 6.1 μm for samples anodized for 60, 90 and 120 minutes, respectively. The average pore diameter of the nanotubes increased from 65 nm (60 minute sample) to 91 nm (90 and 120 minutes samples). Table **1** presents a summary of the physical dimensions of the TiO_2 nanotube arrays prepared at various anodization durations, i.e. average diameter, length, wall thickness, aspect ratio (AR), and geometric surface area factor (G). The aspect ratio and geometric surface area factor were calculated using the following equations:

$$AR = \frac{L}{(D+2w)} \qquad \textbf{[Equation 1]}$$

$$G = \frac{4\pi L(D+w)}{\sqrt{3(D+2w)^2+1}} \quad \textbf{[Equation 2]}$$

where L = nanotube length in nm; D = pore size; w = wall thickness.

The length and pore diameter of the nanotubes were found to be increased with increasing anodization duration due to the continuous field assisted oxidation and dissolution as well as chemical dissolution of the oxide layer, which causes the nanotube array to continue to increase in length with longer anodization times [9, 10].

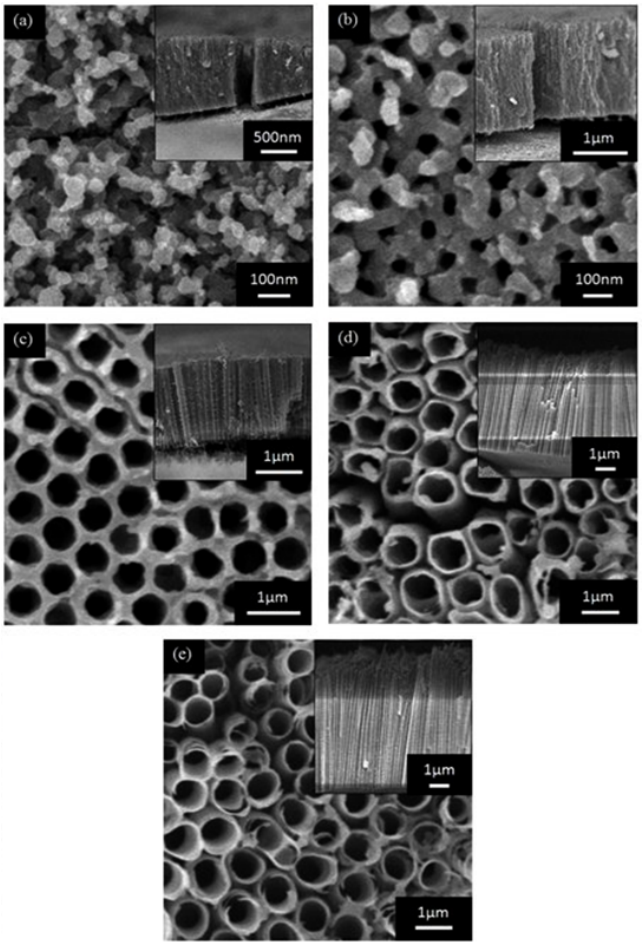

Fig. (1). FESEM images of WO_3-loaded TiO_2 nanotubes obtained with varying anodization duration: (a) 15 min, (b) 30 min, (c) 60 min, (d) 90 min, and (e) 120 min. Insets are the side views of the samples.

The elemental composition of the WO_3-loaded TiO_2 nanotubes films is presented in Table **2**, indicating the presence of Ti, O, W and C. Ethylene glycol present in the electrolyte solution most likely contributed towards the incorporation of carbon on the TiO_2 nanotubes [8]. The W content in the TiO_2 nanotube arrays increased with increasing anodization duration, which is reasonable as more W^{6+} ions are able to migrate and deposit on the titanium anode [11].

Table 2. Energy dispersive X-ray elemental analysis of WO_3-loaded TiO_2 nanotubes obtained with varying anodization duration.

Anodization duration	Atomic %			
	Ti	O	W	C
15 min	33.88	57.31	1.14	7.67
30 min	29.22	62.39	2.20	6.19
60 min	27.89	63.35	2.72	6.04
90 min	27.80	61.34	3.26	7.60
120 min	29.82	62.36	3.50	4.32

3.2. Phase Structure Analysis

Fig. (**2**) presents the diffractograms of the WO_3-loaded TiO_2 nanotube arrays prepared with anodization between 15 to 120 minutes, and annealed at 400 °C under ambient atmospheric conditions for 4 h. The diffraction peaks observed at 25.37°, 38.67°, 48.21°, and 54.10° corresponded to the (101), (112), (200), and (105) crystal planes, respectively, for anatase TiO_2 [JCPDS No. 21-1272]. The increasing crystallinity of the anatase TiO_2 with longer anodization durations was indicated by the intensification of the (101) peak, which is agreeable with FESEM analysis which indicated the formation of thicker and denser TiO_2 nanotube arrays at longer durations [12].

The presence of low-intensity peaks at 23.62° and 29.16° is ascribed to the (020) and (120) crystal planes of the monoclinic WO_3 phase, respectively. These peaks were absent in the sample synthesized at 15 minutes, but were observed in the subsequent samples. This indicates that 15 minutes anodization time is insufficient to allow for significant WO_3 loading. Instead, a minimum anodization time of 30 minutes is necessary for the formation of WO_3 on

Table 1. Physical dimensions of WO_3-loaded TiO_2 nanotubes obtained with varying anodization duration.

Anodization Duration	Diameter (nm)	Length (μm)	Wall thickness (nm)	Aspect Ratio	Geometric surface area factor, G
15 min	-	0.9±0.1	-	-	-
30 min	50±3.5	1.6±0.1	40±1.5	12.31	62.82
60 min	65±2.8	1.8±0.3	24±2.1	15.93	92.02
90 min	91±8.5	5.2±0.2	15±1.6	42.98	274.14
120 min	91±7.5	6.1±0.2	12±0.8	53.04	345.68

TiO_2. Alternatively, the XRD analysis was not sensitive enough to detect WO_3 at low concentrations (<3 at% from EDX analysis) within the TiO_2 lattice due to the nearly similar ionic radius of W^{6+} and Ti^{4+} [13, 14].

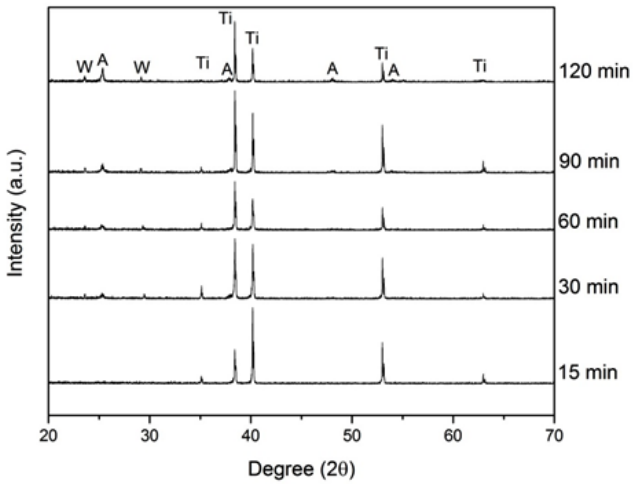

Fig. (2). X-ray diffraction patterns of WO_3-loaded TiO_2 nanotubes produced at different anodization duration.

3.3. Raman Analysis

Raman spectroscopy was conducted to confirm the presence of WO_3 and phase structure of WO_3-loaded TiO_2 nanotube films as presented in Fig. (**3**). The Raman spectra of WO_3-loaded TiO_2 nanotube films feature five characteristic peaks at 145, 198, 396, 518, and 639 cm^{-1}. The strong peak at 145 cm^{-1} corresponds to the E_g phonon of the anatase structure and B_{1g} phonon of the rutile structure. The remaining peaks at 198, 396, 518, and 639 cm^{-1} are attributed to the E_g, B_{1g}, B_{1g}, and E_g modes of the anatase phase, respectively. Thus, the identity of the samples prepared in this study corresponds well with the anatase phase of TiO_2 [12, 15]. The increase in the intensity of anatase peaks with increasing anodization time corresponds to the development and growth of TiO_2 nanotubes as anodization duration is increased. As such, the lower intensity of anatase peaks for sample produced at 15 minutes corresponded with the formation of short and small nanotubes. The sample produced at 120 minutes showed the highest intensity of anatase peaks, corresponding with the formation of a thick and dense TiO_2 layer observed in the FESEM images. The phonon modes for WO_3 were not apparent in the Raman spectrum; WO_3 possesses peak positions at 327, 714, and 804 cm^{-1}, which overlap with Raman peaks arising from anatase TiO_2 [4].

3.4. Optical Properties Analysis

The optical absorption is a key factor in photocatalysis performance. UV-vis DRS is the key characterization technique to study the light absorption properties of materials because it can display the drift, accumulation and recombination of photogenerated carriers as well as useful in estimating the energy band gap (E_{bg}) of the samples. Thus, in this research, the effect of WO_3 doping on the optical absorption properties of TiO_2 nanotubes was investigated using UV-vis DRS.

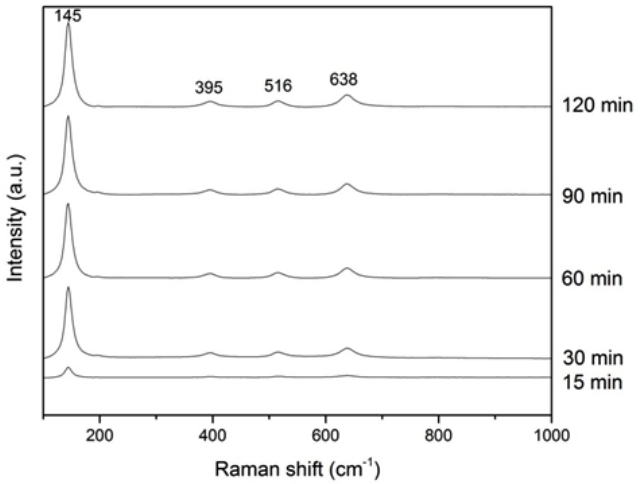

Fig. (3). Raman spectrum of WO_3-loaded TiO_2 nanotubes produced at different anodization durations.

Fig. (**4**) shows the optical absorption patterns of WO_3-loaded TiO_2 and pure TiO_2 nanotube films. Both the WO_3-loaded TiO_2 and pure TiO_2 nanotube films show excellent absorption performance in the UV range. Furthermore, in the whole UV-vis light region, WO_3-loaded TiO_2 nanotubes exhibit higher light absorbance than pure TiO_2 nanotubes and show a red shift in the absorption edges [12, 15]. The greater light absorption in the visible range for the WO_3-loaded TiO_2 sample may be attributed to the WO_3 working synergistically with TiO_2 to enhance absorption efficiency.

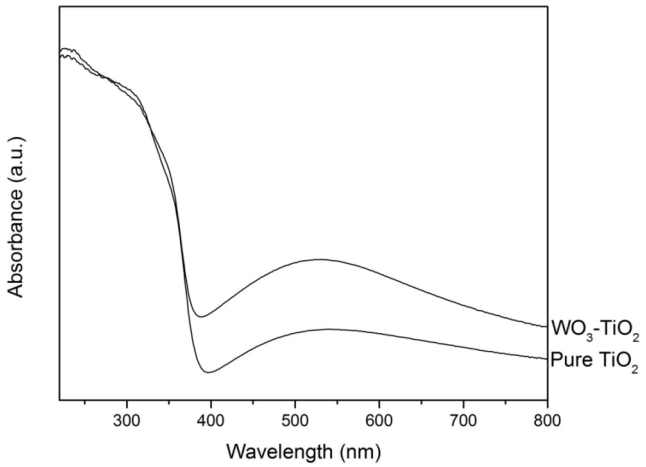

Fig. (4). Absorption patterns of WO_3-loaded TiO_2 nanotubes and pure TiO_2 nanotubes synthesized at duration of 120 minutes.

The band gap energy values of pure TiO_2 nanotubes and WO_3-loaded TiO_2 nanotubes were estimated with the Kubelka-Munk function using the plot of $(\alpha h\nu)^{1/2}$ versus $h\nu$ as shown in Figures 5 and 6 respectively. According to Fig. (**5**), the band gap energy of pure TiO_2 nanotubes was estimated to be 2.84 eV, which was significantly lower compared to the theoretical band gap value of 3.2 eV for TiO_2. The reduction in band gap may be attributed to carbon doping of the TiO_2 nanotubes, whereby the valence band edge of TiO_2 was likely to be shifted upwards as a result of orbital mixing between the delocalized p state of the carbon species

with the 2p orbital of the oxygen species in the valence band of TiO_2 [8, 16]. The band gap energy decreased progressively to 2.72 eV for the WO_3-loaded TiO_2 nanotubes as shown in Fig. (**6**). This finding suggests that the conduction band of the TiO_2 nanotubes was reformed in the presence of W^{6+} ions [17, 18]. Band gap narrowing is observed due to the presence of W^{6+} ions, which introduced impurity energy levels below the Ti conduction band, thereby photons with lower energy may be able to excite electrons from the valence band to these impurity levels. This result also shows that incorporation of WO_3 into TiO_2 would shift the light absorption threshold toward the visible light region and increase the light absorption ability [16].

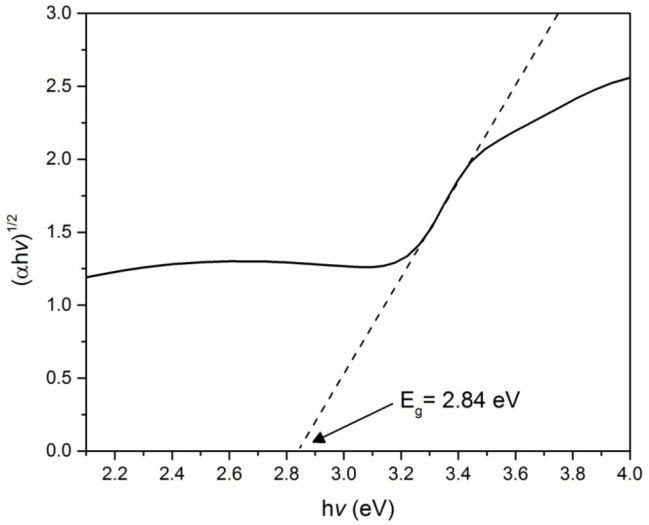

Fig. (5). Plot of $(\alpha h\nu)^{1/2}$ versus hν employed to calculate the band gap value of pure TiO_2 nanotubes synthesized at 120 minutes.

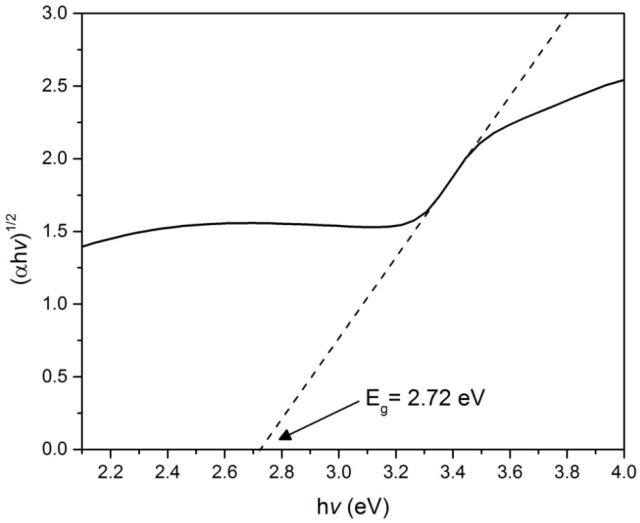

Fig. (6). Plot of $(\alpha h\nu)^{1/2}$ versus hν employed to calculate the band gap value of WO_3-loaded TiO_2 nanotubes synthesized at 120 minutes.

3.5. XPS Analysis

The elemental composition and oxidation state of WO_3-loaded TiO_2 nanotube films were investigated using XPS, and compared with the pure TiO_2 sample. Fig. (**7**) shows the XPS broad survey spectra of WO_3-loaded TiO_2 and pure TiO_2 nanotube films. The presence of W was indicated in the XPS spectrum of the WO_3-loaded TiO_2 sample, along with Ti, O and C elements, indicating that WO_3 was successfully loaded onto the nanotubes.

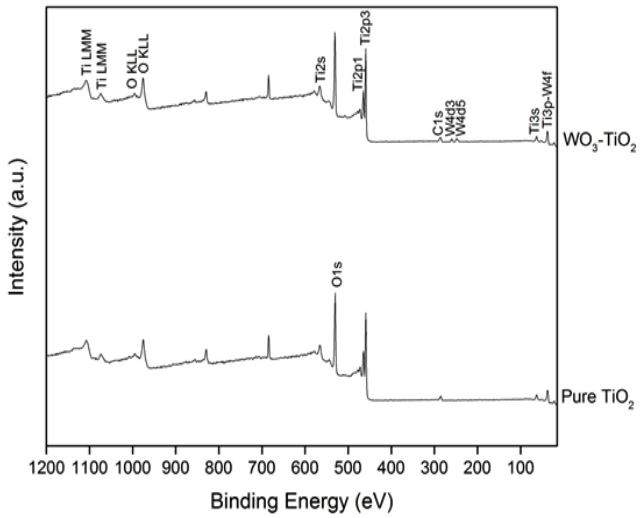

Fig. (7). XPS survey spectra of WO_3-loaded TiO_2 nanotubes and pure TiO_2 nanotubes.

The pure TiO_2 nanotubes possessed characteristic peaks at 459.0 and 464.8 eV (Fig. **8**), which corresponds to the binding energies of $Ti2p_{3/2}$ and $Ti2p_{1/2}$. The hybridization of WO_3 with TiO_2 caused the $Ti2p_{3/2}$ and $Ti2p_{1/2}$ binding energy to increase to 459.6 and 465.4 eV, respectively. The formation of the W-O-Ti bond during the hybridization of WO_3 with TiO_2 has been postulated to proceed through the diffusion of W^{6+} ions into the TiO_2 lattice and displacement of Ti^{4+}, resulting in the contraction of TiO_2 unit cells [10, 19].

The XPS spectrum of the O1s region indicated the presence of Ti-O (530.1 eV) and hydroxyl –OH groups (531.8 eV) (Fig. **9**) [20]. The Ti-O binding energy increased from 530.1 to 530.7 eV with the incorporation of WO_3 on the TiO_2 nanotube arrays, indicating the formation of the W–O–Ti bond from Ti–O and W–O. The intensity of the peak assigned to the –OH group increased with the incorporation of WO_3 [10, 19].

Fig. (**10**) illustrates the C1s binding energy of the pure and WO_3-loaded TiO_2 samples. The peaks at 284.5 and 284.9 eV in pure and WO_3-loaded TiO_2 correspond to the presence of adventitious carbon on the surface of the samples [21]. The peak at 285.7 eV is ascribed to the Ti–C–O bond, which may have originated from the residual ethylene glycol electrolyte on the sample surface. The peak at 288.6 eV is in agreement with other reports on C^{4+}-doped TiO_2 and may be attributed to carbonate species adsorbed on the TiO_2 surface [21, 22]. The presence of C in the nanotube arrays resulted from the adsorption of carbonate species from the pyrogenation of ethylene glycol. The C atom diffused into the TiO_2 crystal structure during the annealing process, forming the Ti-C-O bonds [10, 16].

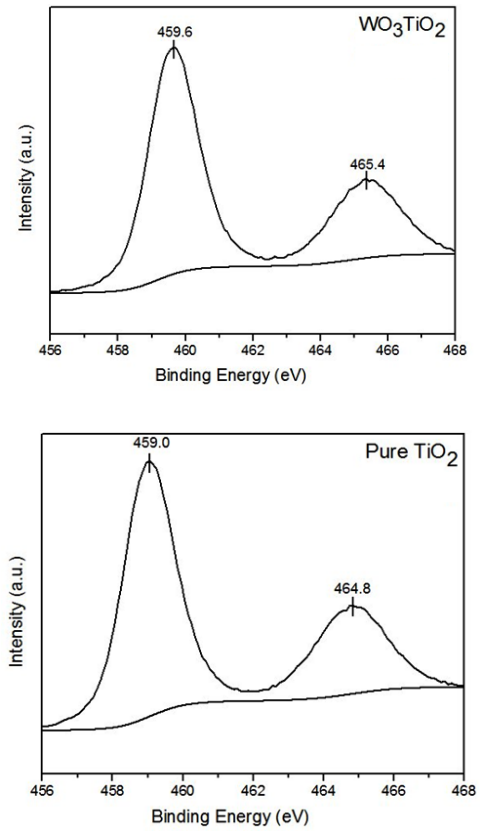

Fig. (8). XPS spectra of Ti2p.

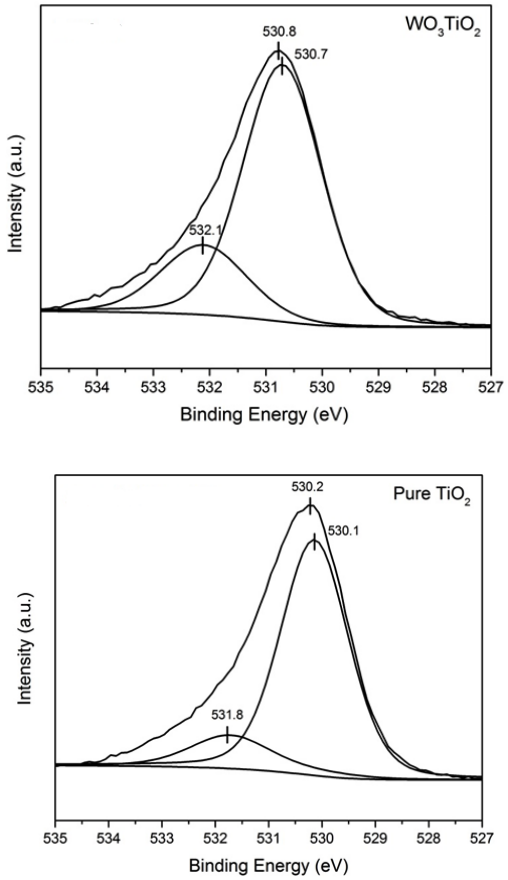

Fig. (9). XPS spectra of O1s.

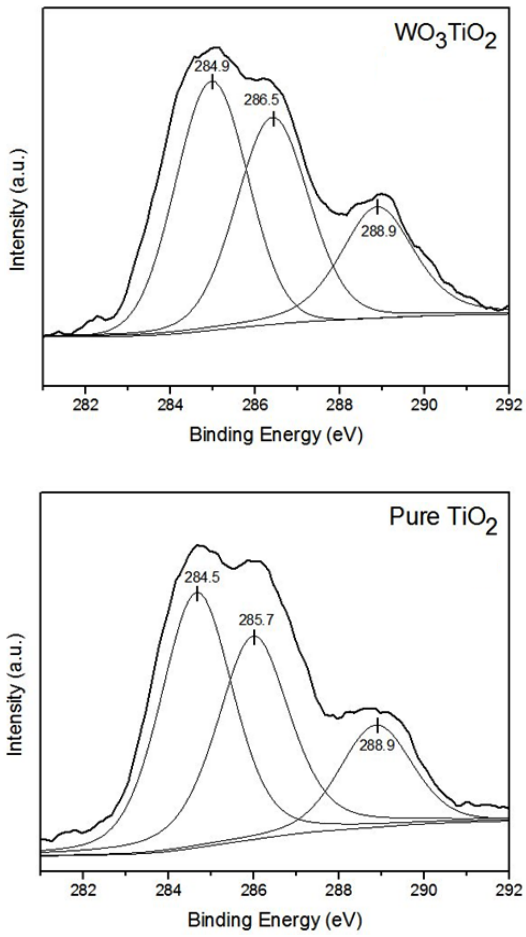

Fig. (10). XPS spectra of C1s.

The XPS peaks characteristic of WO_3 is presented in Fig. (**11**). Peaks at 248.3 and 260.3eV, which correspond to the binding energies of $W4d_{5/2}$ and $W4d_{3/2}$, respectively, were absent in the pure TiO_2 sample but distinctly observed in the annealed WO_3-loaded TiO_2 nanotube arrays. The W4f and Ti3p peaks partially overlap and as such is not distinctly observed in the XPS spectrum. As the W^{6+} ion (74.0 pm) is similar in size to the Ti^{4+} ion (74.5 pm), the formation of W-O-Ti bonds in neutral form is possible by displacement of Ti^{4+} ions with W^{6+} ions using heat treatment [10, 16].

3.6. Photocatalytic Mercury Reduction Performance

It is well known that TiO_2 can reduce aqueous mercury ions under UV illumination. TiO_2 nanotubes, being of nanosize, will have much interaction with mercury ions, which can lead to absorbtion. Thus, photocatalytic reduction of mercury ions leads to conversion to lower oxidation states and probable deposition onto TiO_2 surface as a zerovalent metal [23, 24]. Researchers have shown that mercury reduction involving TiO_2 would be greater under photocatalysis conditions [25]. Therefore, photocatalytic reduction of mercury ions using TiO_2 nanostructures has become a promising mercury removal method. Under UV light, TiO_2 will be photoactive and generate e^-/h^+ pairs (Equation 3). Then, the adsorbed Hg^{2+} ions will be reduced by the e^- on the TiO_2 surface (Equation 4). Fig. (**12**) shows the absorbtion of Hg^{2+} onto the catalyst surface to undergo reduction to Hg^0 [15].

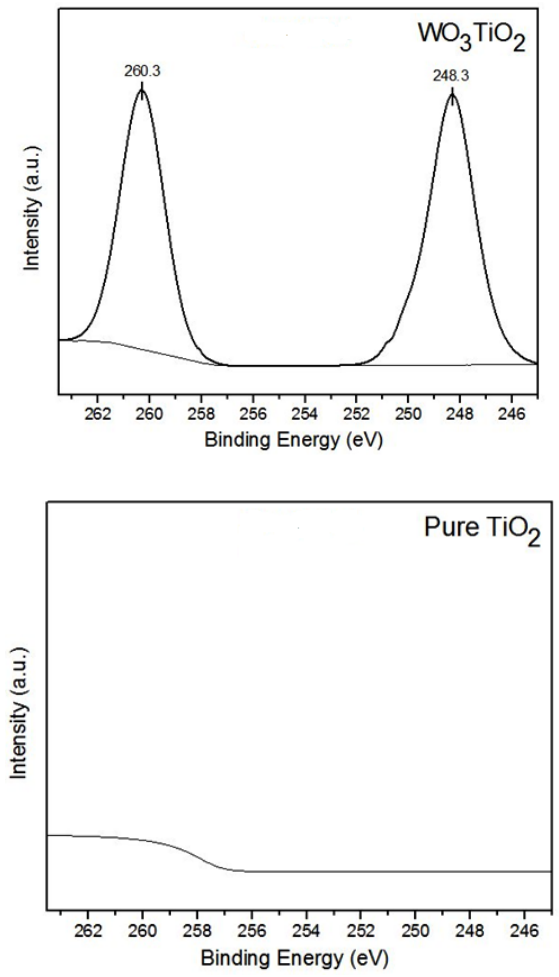

Fig. (11). XPS spectra of W4d.

$TiO_2 + h\nu \rightarrow h^+ + e^-$ [Equation 3]

$Hg^{2+} + 2e^- \rightarrow Hg^0$ [Equation 4]

Based on the results shown in Fig. (**13**) and Table **3**, it may be observed that an increase in anodization duration increased the WO_3-loaded TiO_2 sample's effectiveness towards mercury photoreduction. The WO_3-loaded TiO_2 samples prepared using anodization times of 15, 30, 60 and 90 minutes demonstrated increasing mercury(II) photoreduction efficiency from 11 %, 53 %, 77 % to 87 %, respectively, after two hours of UV irradiation. The WO_3-loaded TiO_2 sample prepared with 120 minutes anodization time demonstrated the highest mercury photoreduction efficiency of 91 %. In this study, an increase in the anodization time increased the aspect ratio and geometric surface area factor of TiO_2 nanotubes, hence larger exposed surface area. TiO_2 nanotube films with larger surface area invariably offer a greater amount of available active surface sites for the interaction between adsorbent and adsorbate, thereby enhancing the rate of mercury adsorption [26]. Other studies have also reported enhanced light scattering effects in TiO_2 samples with high surface area, which may facilitate the generation of photo-induced electron-hole pairs necessary for the reduction of the mercury(II) ion [27, 28]. A control sample of pure TiO_2 nanotubes film was prepared by anodization for 120 minutes using the same electrolyte used to prepare the WO_3-loaded TiO_2 nanotubes, except that a platinum cathode was used to replace the tungsten cathode. Pure TiO_2 nanotube arrays showed a lower efficiency of mercury reduction of 65 % compared to WO_3-loaded TiO_2 nanotube samples prepared by anodization for 60, 90 and 120 minutes. This observation indicates that the coupling between WO_3 and TiO_2 successfully increased charge separation of photogenerated electron-hole pairs by the formation of a potential gradient at the heterojunction [15, 26].

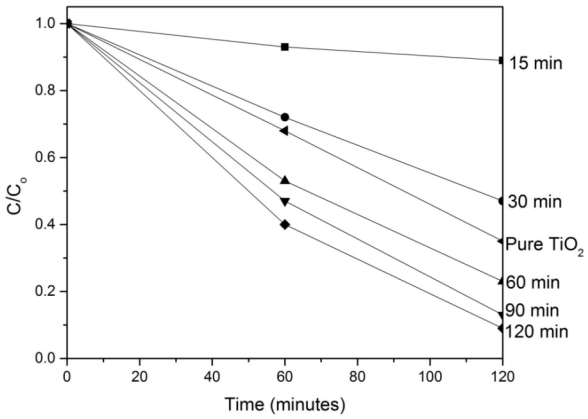

Fig. (13). Reduction of Hg^{2+} by WO_3-loaded TiO_2 nanotubes synthesized at different anodization duration.

A graph of $\ln(C_0/C)$ was plotted against time to evaluate the kinetics of photocatalytic mercury reduction by WO_3-loaded TiO_2 (Fig. **14**). The linear curves in Fig. (**14**) indicate that the photoreduction of mercury proceeded *via* a pseudo-first order reaction, and that the rate constant increased ac-

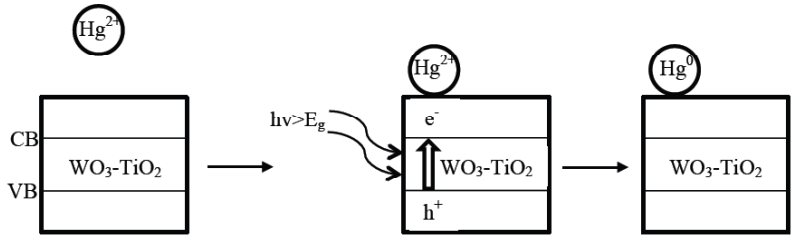

Fig. (12). Photocatalytic reduction of Hg^{2+} ions by WO_3-loaded TiO_2 nanotubes: (a) Hg^{2+} in aqueous medium, (b) absorbtion of Hg^{2+} onto catalyst surface, and (c) reduction of Hg^{2+} ions to Hg^0.

cording to samples prepared with longer anodization time. Using the first-order kinetic equation, $\ln(C/C_0) = kt$, where C_0 is the initial concentration and C is the concentration at time t, the rate constants of the photocatalytic mercury reduction were calculated and presented in Table **4**. The WO_3-loaded TiO_2 nanotubes prepared by anodization for 120 minutes produced the highest rate constant, and therefore the highest rate of mercury(II) photoreduction. It will be beneficial for future study, to predict the total time required for mercury(II) reduction using the present WO_3-loaded TiO_2 sample by plotting a graph of ln (ext/ext_o) versus reaction time, whereby ext = optical transmission at time t and ext_o = initial optical transmission of solution [29].

Table 3. Initial mercury concentration reduced by WO_3-loaded TiO_2 nanotube films prepared by varying the anodization duration.

Sample	Initial mercury concentration reduced
15 min	11%
30 min	53%
60 min	77%
90 min	87%
120 min	91%
Pure TiO_2	65%

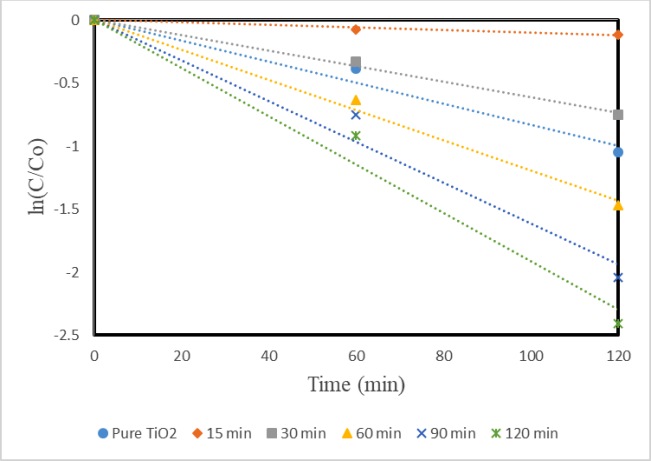

Fig. (14). Pseudo-first-order kinetics for photocatalytic reduction of mercury using WO_3-loaded TiO_2 nanotubes synthesized at different anodization duration.

CONCLUSION

In this study, WO_3-loaded TiO_2 nanotube films were succesfully prepared using a convenient anodization technique for the photoreduction of mercury(II) ions. The investigation of the effect of anodization duration on the formation of WO_3-loaded TiO_2 nanotubes revealed that well-defined structures of WO_3-loaded TiO_2 nanotubes were observed after 30 minutes of anodization in an electrolyte solution containing 0.3 wt% NH_4F dissolved in ethylene glycol, at 40 V. The nanotube length increased with increasing anodization duration, up to approximately 6 µm in length after 120 minutes of anodization. WO_3-loaded TiO_2 nanotubes synthesized at 120 minutes possess larger active surface area and correspond with the highest photocatalytic mercury removal performance, due to an increase in the interaction between adsorbent and adsorbate and more UV photons could be absorbed to generate more electron-hole pairs to reduce Hg^{2+}. The hybridization between WO_3 and TiO_2 was able to increase the light absorption threshold toward the visible light region, as well as suppress electron-hole recombination through the formation of type-III heterojunction.

Table 4. Rate constants for photocatalytic mercury reduction by WO_3-loaded TiO_2 nanotube films prepared by varying the anodization duration.

Sample	Rate constant (k)	R^2
15 min	-0.0010	0.9759
30 min	-0.0061	0.9934
60 min	-0.0119	0.9926
90 min	-0.0161	0.9736
120 min	-0.0191	0.9775
Pure TiO_2	-0.0083	0.9726

ACKNOWLEDGEMENTS

The authors would like to thank thw University of Malaya for funding this research work under Fundamental Research Grant Scheme (FP008-2015A), and Grand Challenge Grant (GC002A-15SBS).

ETHICS APPROVAL AND CONSENT TO PARTICIPATE

Not applicable.

HUMAN AND ANIMAL RIGHTS

No Animals/Humans were used for studies that are base of this research.

CONSENT FOR PUBLICATION

Not applicable.

CONFLICT OF INTEREST

The authors confirm that this article content has no conflict of interest.

REFERENCES

[1] Jaishankar, M.; Tseten, T.; Anbalagan, N.; Mathew, B.; Beeregowda, K.N. Toxicity, mechanism and health effects of some heavy metals. *Interdiscip. Toxicol*., **2014**, *7*(2), 60-72.

[2] Rafati-Rahimzadeh, M.; Rafati-Rahimzadeh, M.; Kazemi, S.; Moghadamnia, A.A. Current approaches of the management of mercury poisoning: Need of the hour. *Daru*., **2014**, *22*, 46.

[3] Cheng, X.; Liu H.; Yu X.; Chen Q.; Li J.; Wang P.; Umar A.; Wang Q. Preparation of highly ordered TiO_2 nanotube array photoelec-

trode for the photoelectrocatalytic degradation of methyl blue: Activity and mechanism study. *Sci. Adv. Mater*., **2013**, *5*(11), 1563-1570.

[4] Roy, P.; Berger, S.; Schmuki, P. TiO_2 nanotubes: Synthesis and applications. *Angew. Chem. Int. Ed. Engl*., **2011**, 50(13), 2904-2939.

[5] Fang, H.; Gao, Y.; Li,G.; An, J.; Wong, P.K.; Fu, H.; Yao, S.; Nie, X.; An, T. Advanced oxidation kinetics and mechanism of preservative propylparaben degradation in aqueous suspension of TiO_2 and risk assessment of its degradation products. *Environ. Sci. Technol*., **2013**, *47*(6), 2704-2712.

[6] Natarajan, T.S.; Natarajan, K.; Bajaj, H.C.; Tayade, R.J. Enhanced photocatalytic activity of bismuth-doped TiO_2 Nanotubes under direct sunlight irradiation for degradation of rhodamine B dye. *J. Nanopart.Res*., **2013**, *15*(5), 1669.

[7] Kitano, M.; Kitano, M.; Kitano, M.; Anpo, M. Recent Developments in titanium oxide-based photocatalysts. *Appl. Catal. A Gen*., **2007**, *325*(1), 1-14.

[8] Lai, C.W.; Sreekantan, S. Single step formation of C-TiO_2 nanotubes: Influence of applied voltage and their photocatalytic activity under solar illumination. Int. J. Photoenergy, **2013**, *2013*, 1-8.

[9] Leghari, S.A.K.; Shamaila, S.; Chen, F.; Zhang, J. WO_3/TiO_2 composite with morphology change via hydrothermal template-free route as an efficient visible light photocatalyst. Chem. Eng. J., **2011**, *166*(3),906-915.

[10] Lai, C.W.; Sreekantan S. Optimized sputtering power to incorporate WO_3 into C–TiO_2 nanotubes for highly visible photoresponse performance. Nano, **2012**, *07*(06), 1250051.

[11] Lai, C.W.; Sreekantan S. Preparation of hybrid WO_3–TiO_2 nanotube photoelectrodes using anodization and wet impregnation: improved water-splitting hydrogen generation performance. *Int. J. Hydrogen Energy*, **2013**, 38(5), 2156-2166.

[12] Lee, W. H.; Lai C.W.; Abd. Hamid S.B. One-step formation of WO_3-Loaded TiO_2 nanotubes composite film for high photocatalytic performance. *Materials*, **2015**, *8*(5), 2139-2153.

[13] Lai, C.W.; Sreekantan, S.; Sun, P.E.; Krengvirat W. Preparation and photoelectrochemical characterization of WO_3-loaded TiO_2 nanotube arrays via radio frequency sputtering. E*lectrochim. Acta*, **2012**, *77*, 128-136.

[14] Lai, C.W.; Sreekantan, S.; E, P.S. Effect of radio frequency sputtering power on W-TiO_2 nanotubes to improve photoelectrochemical performance. *J. Mater.Res*., **2012**, *27*(13), 1695-1704.

[15] Lee, W.H.; Lai C.W.; Abd. Hamid, S.B. *In situ* anodization of WO_3-decorated TiO_2 nanotube arrays for efficient mercury removal. *Materials*, **2015**, *8*(9), 5270-5714.

[16] Lai, C.W.; Sreekantan S. Study of WO_3 incorporated C-TiO_2 nanotubes for efficient visible light driven water splitting performance. *J. Alloys Compd.*, **2013**, *547*, 43-50.

[17] Momeni, M.M.; Ghayeb, Y.; Davarzadeh, M. Electrochemical construction of different titania–tungsten trioxide nanotubular composite and their photocatalytic activity for pollutant degradation: A recyclable photocatalysts. *J. Mater. Sci. Mater. Electron.*, **2015**, *26*(3), 1560-1567.

[18] Xin Y.; Liu, H.; Liu, Y.; Ma, D.; Chen, Q. Composition and photoelectrochemical properties of WO_3/TNAs photoelectrodes fabricated by *in situ* electrochemical method. *Electrochim. Acta*, **2013**, *104*, 308-313.

[19] Lai, C.W.; Sreekantan, S. Heat treatment effects of WO_3-loaded TiO_2 nanotubes with enhanced water splitting hydrogen generation. *Mate.r Sci. Semicond. Process*., **2013**, *16*, 947-954.

[20] Hussain, H.; Tocci, G.; Woolcot, T.; Torrelles , X.; Pang, C.L.; Humphrey, D.S.; Yim, C.M.; Grinter, D.C.; Cabailh, G.; Bikondoa, O.; Lindsay, R.; Zegenhagen, J.; Michaelides, A.; Thornton, G. Structure of a model TiO_2 photocatalytic interface. *Nat. Mater*., **2016**, *16*, 461-466.

[21] Chen, C.; Long, M.; Zeng, H.; Cai, W.; Zhou, B.; Zhang, J.; Wu, Y.; Ding, D.; Wu, D. Preparation, characterization and visible-light activity of carbon modified TiO_2 with two kinds of carbonaceous species. *J. Mol. Catal. A: Chem*., **2009**, *314*(1–2), 35-41.

[22] Neumann, B.; Bogdanoff, P.; Tributsch, H.; Sakthivel, S.; Kisch, H. Electrochemical mass spectroscopic and surface photovoltage studies of catalytic water photooxidation by undoped and carbon-doped titania. *J. Phys. Chem. B*., **2005**, *109*(35), 16579-16586.

[23] Suriyawong, A.; Smallwood, M.; Li, Y.; Ye Z.; Biswas P. Mercury capture by nano-structured titanium dioxide sorbent during coal combustion: Lab-scale to pilot-scale studies. *AEROSOL* AIR QUAL. RES., **2009**, *9*(4), 394-403.

[24] Tsai, C.Y.; Kuo, T.H.; His, H.C. Fabrication of Al-doped TiO_2 Visible-light photocatalyst for low-concentration mercury removal. *Int. J.* Photoenergy, **2012**, *2012*, 1-8.

[25] Byrne, H.E.; Mazyck, D.W. Removal of trace level aqueous mercury by adsorption and photocatalysis on silica–titania composites. *J. Hazard. Mater*., **2009**, *170*(2-3), 915-919.

[26] Yu, C.; Yu, J.; Zhou, W.; Yang, K. WO3 Coupled p-TiO_2 photocatalysts with mesoporous structure. *Catal. Lett*., 2010, *140*(3), 172-183.

[27] Skubal, L.R.; Meshkov N.K. Reduction and removal of mercury from water using arginine-modified TiO_2. *J. Photochem. Photobiol. A Chem*., **2002**, *148*(1-3), 211-214.

[28] Nischk, M.; Mazierski, P.; Gazda, M.; Zaleska, A. Ordered TiO_2 Nanotubes: The effect of preparation parameters on the photocatalytic activity in air purification process. *Appl. Catal. B.*, **2014**, *144*, 674-685.

[29] Hunge, Y.M.; Mahadik M.A.; Moholkar A.V.; Bhosale, C.H. Photoelectrocatalytic degradation of oxalic acid using WO3 and stratified WO3/TiO2 photocatalysts under sunlight illumination. *Ultrason. Sonochem*., **2017**, *35*(Part A), 233-242.